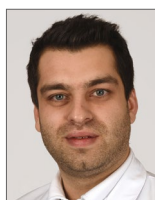


Diagnostic performance of a Lattice Boltzmann-based method for CT-based fractional flow reserve



Andreas A. Giannopoulos^{1,2}, MD; Anji Tang¹, BA; Yin Ge¹, MD; Michael K. Cheezum¹, MD; Michael L. Steigner¹, MD; Shinichiro Fujimoto³, MD, PhD; Kanako K. Kumamaru³, MD, PhD; Dante Chiappino⁴, MD; Daniele Della Latta⁴, MS; Sergio Berti⁴, PhD; Sara Chiappino⁴, MD; Frank J. Rybicki⁵, MD, PhD; Simone Melchionna⁶, PhD; Dimitrios Mitsouras^{1,5*}, PhD

1. Brigham and Women's Hospital, Harvard Medical School, Boston, MA, USA; 2. University Hospital Zurich, Zurich, Switzerland; 3. Juntendo University Graduate School of Medicine, Tokyo, Japan; 4. Ospedale "G. Pasquinucci", Massa, Italy; 5. University of Ottawa Faculty of Medicine, Ottawa, ON, Canada; 6. EXA Corporation, Burlington, MA, USA

KEYWORDS

- clinical research
- fractional flow reserve
- multislice computed tomography (MSCT)
- non-invasive imaging

Abstract

Aims: Fractional flow reserve (FFR) estimated from coronary computed tomography angiography (CT-FFR) offers non-invasive detection of lesion-specific ischaemia. We aimed to develop and validate a fast CT-FFR algorithm utilising the Lattice Boltzmann method for blood flow simulation (LBM CT-FFR).

Methods and results: Sixty-four patients with clinically indicated CTA and invasive FFR measurement from three institutions were retrospectively analysed. CT-FFR was performed using an onsite tool interfacing with a commercial Lattice Boltzmann fluid dynamics cloud-based platform. Diagnostic accuracy of LBM CT-FFR ≤ 0.8 and percent diameter stenosis $>50\%$ by CTA to detect invasive FFR ≤ 0.8 were compared using area under the receiver operating characteristic curve (AUC). Sixty patients successfully underwent LBM CT-FFR analysis; 29 of 73 lesions in 69 vessels had invasive FFR ≤ 0.8 . Total time to perform LBM CT-FFR was 40 ± 10 min. Compared to invasive FFR, LBM CT-FFR had good correlation ($r=0.64$), small bias (0.009) and good limits of agreement (-0.223 to 0.206). The AUC of LBM CT-FFR (AUC=0.894, 95% confidence interval [CI]: 0.792-0.996) was significantly higher than CTA (AUC=0.685, 95% CI: 0.576-0.794) to detect FFR ≤ 0.8 ($p=0.0021$). Per-lesion specificity, sensitivity, and accuracy of LBM CT-FFR were 97.7%, 79.3%, and 90.4%, respectively.

Conclusions: LBM CT-FFR has very good diagnostic accuracy to detect lesion-specific ischaemia (FFR ≤ 0.8) and can be performed in less than one hour.

*Corresponding author: Applied Imaging Science Lab, Brigham and Women's Hospital, 75 Francis Street, Boston, MA 02115, USA. E-mail: dmitsouras@alum.mit.edu

Abbreviations

AUC	area under the curve
CAD	coronary artery disease
CFD	computational fluid dynamics
CI	confidence interval
CT	computed tomography
CTA	computed tomography angiography
CTP	computed tomography perfusion
DS	diameter stenosis
FFR	fractional flow reserve
GPU	graphics processing unit
ICA	invasive coronary angiography
LBM	Lattice Boltzmann method
PET	positron emission tomography
ROC	receiver operating characteristic
ROI	region of interest
SCCT	Society of Cardiovascular Computed Tomography
SPECT	single-photon emission computed tomography
3D	three-dimensional

Introduction

Coronary computed tomography angiography (CTA) is used to exclude anatomically obstructive coronary artery disease (CAD) in low- to intermediate-risk symptomatic patients¹. Numerous studies have demonstrated high correlation of anatomic lesion severity identified by CTA and invasive coronary angiography (ICA), and a high negative predictive value to exclude obstructive CAD in patients with both stable² and acute chest pain³. However, CTA has limited specificity to predict the haemodynamic significance of CAD. Approximately half of obstructive lesions ($\geq 50\%$ lumen diameter stenosis) determined by CTA do not cause ischaemia⁴. Traditionally, further functional testing is required to determine the haemodynamic significance of obstructive CAD⁵. This includes exercise treadmill testing, single-photon emission computed tomography (SPECT)⁶, positron emission tomography (PET)⁷, stress magnetic resonance imaging, stress echocardiography and, more recently, CT perfusion (CTP)⁸.

The reference standard to identify lesion-specific ischaemia is invasive fractional flow reserve (FFR) performed at ICA⁹. FFR is superior to anatomical measures of CAD for guiding revascularisation⁹⁻¹⁴. FFR_{CT} (HeartFlow Inc., Redwood City, CA, USA) estimates FFR from a standard coronary CTA exam with excellent accuracy to demonstrate lesion-specific ischaemia as defined by invasive FFR ≤ 0.8 ¹⁵⁻¹⁷. In stable symptomatic patients with suspected CAD and no prior myocardial infarction or coronary revascularisation, FFR_{CT} can serve as a gate-keeper to ICA with cost savings and improved quality of life compared to the current standard of care¹⁸.

Other techniques to estimate invasive FFR from CTA have been developed¹⁹⁻²¹, in part to improve FFR_{CT} computation times and render them compatible with clinical workflow. To date, this has involved simplifying the time-intensive computational fluid dynamics (CFD) computations underlying FFR estimation from

CTA data. CFD is used to solve the Navier-Stokes equations of blood flow in the three-dimensional (3D) coronary lumen extracted from CTA under simulated hyperaemic conditions. 3D CFD yields the pressure drop across a coronary lesion, from which FFR can be calculated²². Simplifications to date involve reduction of the 3D computational problem to a (primarily or fully) single-dimensional^{19,20,23} or two-dimensional²¹ anatomic model to decrease computation time.

The Lattice Boltzmann method (LBM) is an alternative computational technique to discretise the 3D blood flow equations²⁴⁻²⁶. It can be used similarly to traditional CFD to solve the 3D blood flow in a coronary artery²⁷ and has been used to derive the pressures required for FFR estimation²⁸. Its main advantage in comparison to traditional CFD techniques is that it allows extremely efficient distribution of the CFD computations amongst multiple computer processors²⁹.

We report the validation of a CT-FFR algorithm utilising the LBM CFD technique (LBM CT-FFR) in a multinational patient cohort collected retrospectively from three independent institutions in Asia, Europe and the United States of America. The technique is fully automated and reconstructs blood flows via a commercial fluid dynamics LBM solver that offers high computational accuracy and automated parallelisation of the computation³⁰⁻³².

Methods

STUDY POPULATION

The institutional review board of each participating institution approved this retrospective study and waived the requirement for written informed consent. The study included 64 patients with neither prior stent implantation nor coronary artery bypass graft referred for coronary CTA and who subsequently underwent ICA with FFR measurement in ≥ 1 vessel based on the standard-of-care patient management algorithm at each institution. Twenty-one consecutive patients were included from one institution in Japan, twenty consecutive patients were included from a second institution in Italy, and twenty-three consecutive patients were included from a third institution in the USA.

CT ANGIOGRAPHY

Coronary CTA was performed in all institutions in accordance with the recommendations of the Society of Cardiovascular Computed Tomography (SCCT)³³. Patients were imaged with a variety of scanners with a minimum of 64-detector row CT, including Aquilion™ 64 and Aquilion ONE™ (Toshiba Medical Systems Corporation, Otawara, Japan), Discovery™ 64 (General Electric Healthcare, Chicago, IL, USA) and SOMATOM Definition (Siemens Healthcare, Erlangen, Germany). Patients with heart rate > 65 beats/min received oral or intravenous beta-blockade, and all patients received 0.4 mg sublingual nitroglycerine before imaging.

Iodinated contrast medium was injected with a power injector into an antecubital vein at flow rates of 4.5-6 ml/sec. The type of contrast medium was specific to each institution and included Omnipaque 300 and 350 (Daiichi Sankyo Inc., Tokyo,

Japan), Iopromide 370 (Bayer AG, Leverkusen, Germany), and Iomeprol-400 and Isovue-370 (Bracco Diagnostics, Milan, Italy). At all institutions, CT acquisition (either retrospectively or prospectively gated) was timed by bolus tracking in the descending aorta. All studies used ECG-based current modulation and images were acquired with 0.35-0.45 sec gantry rotation time and 100-120 kVp tube potential. Images were reconstructed at 0.5-0.625 mm slice thickness with 0.25-0.4 mm spacing.

CTA scans were interpreted at the institution at which they were acquired. CAD severity was categorised as $\leq 50\%$, 51-75%, and $>75\%$, using an 18-segment model according to SCCT guidelines³⁴ in images at the cardiac phase deemed to be least affected by motion. Lesions with $\leq 50\%$ diameter stenosis (DS) were considered non-obstructive, and those with $>50\%$ DS were considered obstructive³⁵.

INVASIVE CORONARY ANGIOGRAPHY

Invasive coronary angiography was performed according to local standard clinical practice at each institution via a femoral or radial approach. Invasive FFR was performed at the discretion of individual operators when clinically appropriate and according to local practice. The pressure wire (Verrata[®] pressure guide wire [Philips Volcano, Philips Healthcare, Amsterdam, the Netherlands] or PressureWire[™] Aeris[™] guidewire [St. Jude Medical, St. Paul, MN, USA]) was calibrated and equalised with the aortic pressure before being placed distal to the stenosis and in the distal third of the coronary artery being interrogated. Hyperaemia was induced by intravenous administration of either adenosine or papaverine hydrochloride. FFR was calculated by dividing the mean coronary pressure measured with the pressure sensor placed distal to the stenosis by the mean aortic pressure measured through the guide catheter at steady-state hyperaemia.

CT-FFR ALGORITHM

A stand-alone automated CT-FFR algorithm was developed to estimate FFR from CTA. The algorithm calculated the blood flow velocities and pressures using an LBM CFD model that includes the 3D anatomy of the coronary arteries extracted from the CT angiogram and that considers both the physical characteristics of blood and a physiologic model of the coronary circulation.

Three-dimensional models of the left and right coronary trees were generated from coronary CTA images using proprietary, purpose-developed software (EXA Corporation, Burlington, MA, USA) to segment coronary arteries using methods that rely on contrast enhancement³⁶ and surrounding plaque characteristics³⁷. Specifically, the algorithm requires manual identification of the coronary ostia. Based on those seed points, voxels are automatically segmented to belong to the coronary lumen via region growing that automatically adjusts for the local contrast opacification³⁶. The algorithm allows additional seed points to be added by the operator, e.g., to guide the algorithm to segment additional relevant branches or distal segments if those were not automatically segmented. Following voxel segmentation, vessel centrelines and

cross-sectional regions of interest (ROIs) enclosing the lumen were automatically calculated. Distal segments with a cross-sectional diameter <1 mm were automatically trimmed, with manual override if desired. Finally, cross-sectional ROIs were adjusted by manual editing, if desired.

Blood flow simulations were performed using a Lattice Boltzmann fluid dynamics method, modelling blood as a Newtonian fluid. The LBM solves the equations governing fluid dynamics by means of a kinetic formulation, treating blood as a group of pseudo-particles that evolve explicitly in time over a Cartesian grid. This is in contrast to traditional CFD, which decomposes the lumen into small finite volumes and iteratively balances the integral equations of velocity, pressure, energy and other relevant properties for conservation across the collection of finite volumes. The commercial PowerFLOW[®] platform (EXA Corporation) was used for the LBM solver. This platform has built-in partitioning of the blood flow computational grid for parallel computing, and enables a speed-up of the computation that is proportional to the number of computer processing units available. The processing units ("cores") can be ordinary computer processors or specialised hardware such as graphics processing units (GPUs), installed either locally or remotely, e.g., in a "cloud" computing environment. In this work, we performed the calculation on 388 cores of a web-based cloud computing facility hosted by IBM (ExaCLOUD).

A physiologic model was used to estimate each patient's hyperaemic blood flow conditions incorporating blood flow rates established by the Prediction of Progression of Coronary Artery Disease and Clinical Outcome Using Vascular Profiling of Shear Stress and Wall Morphology (PREDICTION) trial³⁸. Flow distribution in each coronary artery branch was based on Murray's law³⁹.

Mean pressure distal to the interrogated lesion was obtained from the LBM blood flow simulation in the vessel location matching the invasive FFR measurement based on interpretation of the ICA images recording pressure wire position. Matching was blinded to the invasive FFR measurement. LBM CT-FFR values were then calculated by dividing the mean pressure distal to the coronary lesion by the mean aortic pressure.

STATISTICAL ANALYSIS

Statistical analyses were performed in Stata v9.2 (StataCorp, College Station, TX, USA). LBM CT-FFR values for each lesion interrogated by invasive FFR were first correlated to the invasive FFR measurements using the Pearson correlation coefficient and Bland-Altman analysis to assess the bias and limits of agreement between LBM CT-FFR and invasive FFR measurements. The receiver operating characteristic (ROC) area under the curve (AUC) was then used to assess the diagnostic accuracy of LBM CT-FFR and CTA ($\leq 50\%$ diameter stenosis cut-off) to detect lesion-specific ischaemia as defined by an invasive FFR measurement ≤ 0.8 . All models accounted for data clustering for multiple arteries examined in the same patient. The ROC AUCs were compared using the DeLong method⁴⁰; a p-value of <0.05 was considered to be statistically significant. Point estimates of

diagnostic accuracy, sensitivity, and specificity to detect an invasive FFR ≤ 0.8 were finally calculated for LBM CT-FFR ≤ 0.8 and CTA $>50\%$ diameter stenosis.

For 18 randomly selected patients, LBM CT-FFR was additionally performed by a second operator to assess method reproducibility. Agreement of the continuous LBM CT-FFR measurements between the two readers was first assessed using Pearson correlation and Bland-Altman limits of agreement, as well as the intraclass correlation coefficient using a two-way random effects model. Second, agreement of the categorical determination of lesion haemodynamic significance (determined by LBM CT-FFR ≤ 0.8) between operators was assessed using the Cohen kappa statistic.

Results

Of the 64 patients, four were excluded due to inability to perform LBM CT-FFR due to failure of the segmentation method secondary to inadequate CTA image quality. Patient characteristics for the remaining 60 patients are provided in **Table 1**. Invasive FFR measurements were performed in 73 lesions in 69 vessels at a median time of 23 days (interquartile range: 6 to 58 days) after CTA (**Table 2**). Twenty-nine lesions (40%) had a haemodynamically significant invasive FFR measurement ≤ 0.8 (**Table 2**).

The average total time required to perform the LBM CT-FFR calculation, starting from initiating loading of the image data set and including segmentation, was 40 ± 10 min. There was strong

Table 1. Study population characteristics.

Demographics (N=60)	
Gender (male)	45 (75%)
Age (years)	61.5 \pm 9.6
Height (cm)	169.3 \pm 10.7
Weight (kg)	77.6 \pm 17.8
BMI (kg/cm ²)	26.8 \pm 3.7
CAD risk factors/related history	
Diabetes mellitus	21 (35%)
Hypertension	40 (67%)
Hyperlipidaemia	34 (57%)
Smoking	9 (18%)
Prior myocardial infarction	1 (2%)
Prior PCI	0 (0%)
Invasive FFR measurements	
LAD	55 (75%)
LCx	10 (14%)
RCA	5 (7%)
Other	3 (4%)
CT indication	
Angina	30 (50%)
Abnormal/equivocal test	25 (42%)
Pre-op evaluation	2 (3%)
Other	3 (5%)

Table 2. Determination of coronary artery disease in study cohort by each modality.

Vessels interrogated by FFR		69
Lesions interrogated by FFR		73
Lesion CTA characteristics		
Non-obstructive ($\leq 50\%$)		27 (37%)
Obstructive ($>50\%$)		46 (63%)
Calcified		19 (26%)
Complex		38 (52%)
Non-calcified		16 (22%)
Plaque volume	Mild	2 (3%)
	Moderate	15 (21%)
	Severe	56 (77%)
LBM CT-FFR ≤ 0.8		24 (33%)
Lesion coronary angiography characteristics		
Non-obstructive ($\leq 50\%$)		30 (41%)
Obstructive ($>50\%$)		43 (59%)
Invasive FFR ≤ 0.8		29 (40%)
Average FFR		0.81 \pm 0.11
# Lesions with FFR=0.75-0.8		8 (11%)
# Lesions with FFR=0.75-0.85		19 (26%)

correlation between the LBM CT-FFR values and invasive FFR measurements (Pearson's $r=0.6$) and Bland-Altman analysis revealed a small bias of -0.009 and limits of agreement of -0.223 to 0.206 (**Figure 1**). Two example cases are shown in **Figure 2** and **Figure 3**.

The AUC of LBM CT-FFR to detect FFR ≤ 0.8 was 0.894 (95% confidence interval [CI]: $0.792-0.996$) (**Figure 4**). With respect to invasive FFR ≤ 0.8 , LBM CT-FFR analysis identified 23 true positives and 43 true negatives, while there was one false positive and six false negatives. The sensitivity, specificity, and diagnostic accuracy of LBM CT-FFR ≤ 0.8 to detect FFR ≤ 0.8 were 79.3% (95% CI: $66.9-82.6\%$), 97.7% (95% CI: $89.5-99.9\%$) and 90.4% (95% CI: $80.5-93.0\%$), respectively. The AUC of CTA to detect FFR ≤ 0.8 was 0.685 (95% CI: $0.577-0.794$), with a sensitivity, specificity and accuracy of CTA $>50\%$ diameter stenosis of 82.8% (95% CI: $67.6-93.0\%$), 50% (95% CI: $40.0-56.8\%$), and 63% (95% CI: $50.9-71.2$), respectively. The ROC AUC of LBM CT-FFR was significantly higher than that of CTA percent diameter stenosis ($p=0.0021$) (**Figure 4**).

In the 18 patients assessed by two different operators, 22 lesions were analysed of which five had invasive FFR ≤ 0.8 . LBM CT-FFR values were well correlated between operators (Pearson's $r=0.9$), had a low bias of 0.003 , and limits of agreement were -0.088 to 0.094 . The intraclass correlation coefficient was 0.848 (95% CI: $0.730-0.966$) and the Cohen kappa for CT-FFR assessment of haemodynamic significance was $\kappa=1.00$, with both operators' CT-FFR analysis correctly identifying all five haemodynamically significant lesions, with no false positives or false negatives.

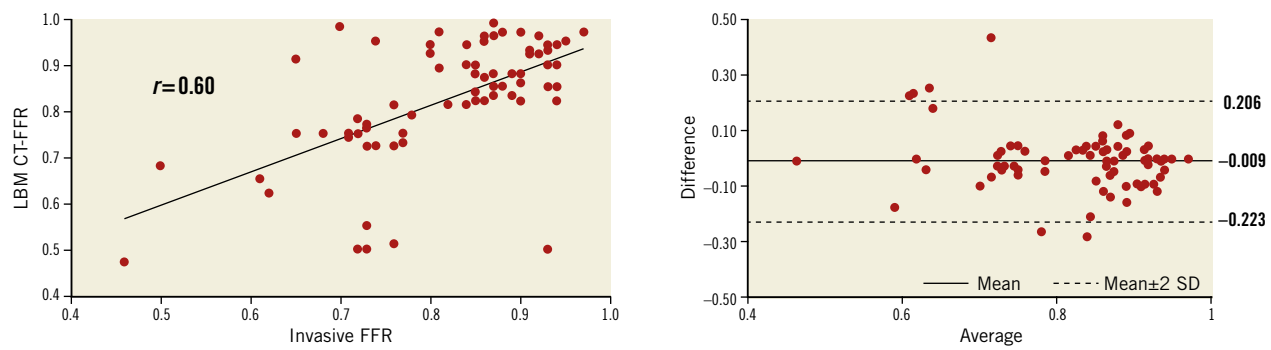


Figure 1. Pearson correlation and Bland-Altman plots of LBM CT-FFR and invasive FFR measurements.

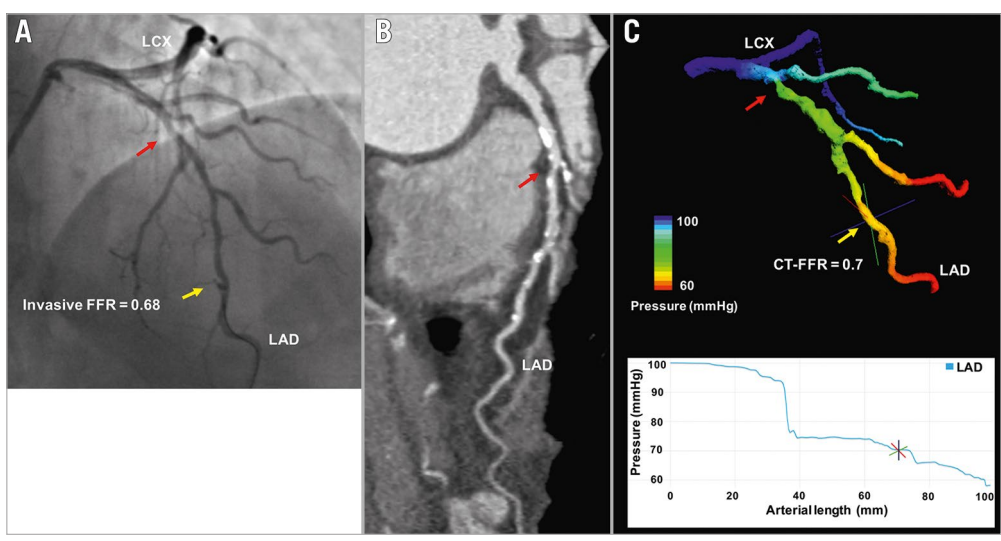


Figure 2. Representative example of LBM CT-FFR estimation in a haemodynamically significant lesion. ICA (A) and CTA (B) of haemodynamically significant mid-LAD lesion with LBM CT-FFR simulation result (C). Red arrow marks the lesion; yellow arrow marks the location of FFR and LBM CT-FFR measurement.

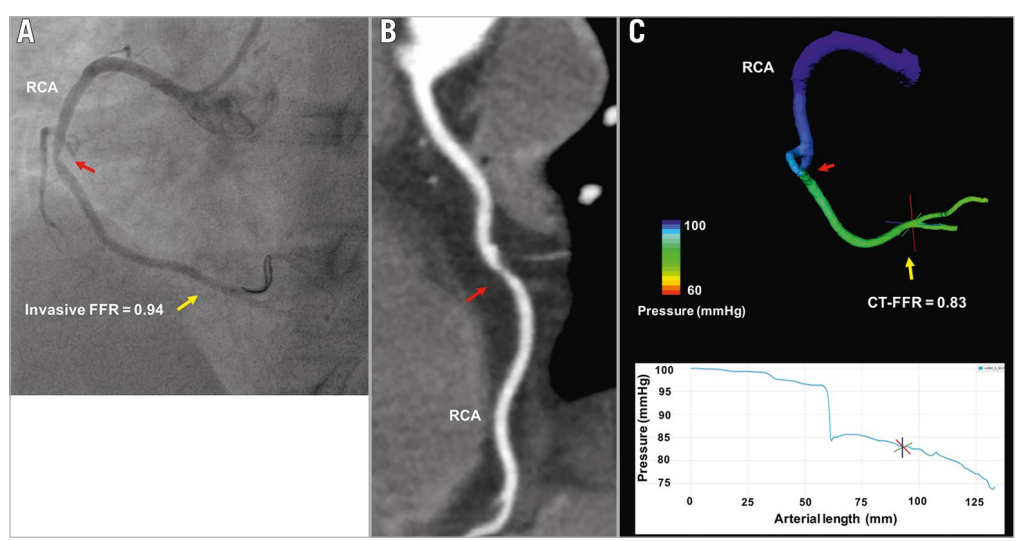


Figure 3. Representative example of LBM CT-FFR estimation in a haemodynamically non-significant lesion. ICA (A) and CTA (B) of non-haemodynamically significant mid-RCA lesion with LBM CT-FFR simulation result (C). Red arrow marks the lesion; yellow arrow marks the location of FFR and LBM CT-FFR measurement.

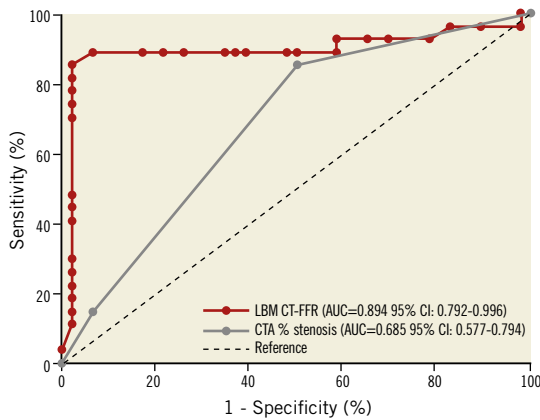


Figure 4. Receiver operating characteristic curves of LBM CT-FFR and CTA to detect invasive FFR ≤ 0.8 .

Discussion

The primary conclusion of this study is that a fast LBM-based CT-FFR algorithm has better diagnostic accuracy to detect an invasive FFR ≤ 0.8 than anatomic lesion severity evaluation by CTA. In our patient cohort, LBM CT-FFR test characteristics were similar to those of previously reported CT-FFR techniques^{15-17,19,21,23}. This includes the correlation between LBM CT-FFR measurements and invasive FFR measurements ($r=0.6$), limits of agreement with invasive FFR (-0.223 to 0.206), and overall diagnostic accuracy (90.4%) and ROC AUC (0.89) to detect lesions with invasive FFR ≤ 0.8 .

The LBM CT-FFR technique ensures 3D accuracy of the hyperaemic blood flow simulation throughout the coronary tree by using a fast commercial, validated LBM solver. This is in contrast to other approaches that employ traditional CFD solvers or that employ “reduced-order” models of the coronary circulation to decrease the computational burden^{19-21,23}.

Some CT-FFR techniques reported to date^{19,21} have only been applied to images acquired on a particular vendor’s hardware, potentially due to vendor-specific CTA image requirements. In contrast, our CT-FFR approach is most similar to the initial FFR_{CT} technology in that it can be applied to coronary CTA images independent of the CT scanner used to acquire them^{16,22}. This option is likely to be useful for institutions with multi-vendor CT platforms. Additionally, LBM CT-FFR enables users to scale the computational resource, and thus reduce turn-around time. The computational resource can be located either on- or off-site depending on the desired investment for computing hardware, potentially enabling the cardiovascular imager to centralise the computation needed to perform CT-FFR interpretation based on each practice’s individual requirements. The latter option affords the opportunity to share the CT-FFR resource not only between individual practice sites, but also between independent practices. Specifically, because of the intrinsic structure of LBM, the CFD accuracy requirement for accurate CT-FFR estimation can be met while the computation is accomplished with a turn-around time that scales down linearly with the number of processors.

The technique was developed to perform blood flow and FFR calculations in a substantially unsupervised fashion, including subdivision (parallelisation) of the computation on all available computer cores to achieve a systematic reduction of the “time-to-solution” with an increasing number of computing resources as necessary for routine clinical workflow. In this study, the segmentation and computation time were roughly 20 minutes each. Further refinements are likely to reduce the segmentation time substantially. Finally, workflow is simplified by using an on-site “front end” for the clinician to perform all image processing and interpretation steps, such as segmentation, and, when the fluid dynamics problem is solved (either “on-” or “off-site”), to manipulate (pan, rotate, zoom) the LBM CT-FFR results on-site similar to other 3D visualisation tools independent of where the computational resource used to perform the simulation is located. The user can quickly view the pressure drop along the length of each artery and report the CT-FFR estimate in a particular location (**Figure 2**, **Figure 3**).

Limitations

We acknowledge several study limitations, particularly the retrospective nature and the relatively small cohort. Test characteristics of LBM CT-FFR reported here are preliminary and will probably change as larger studies are performed and as the method evolves towards better balancing of sensitivity versus specificity, similar to the development of other CT-derived FFR technologies. Importantly, accuracy of the anatomical coronary lumen model may depend on the CTA image quality and degree of calcification. The majority of patients in our cohort did not have a calcium scoring study and thus our results may not be generalisable to patients with a high Agatston score. Although there were differences in CTA and FFR protocols among the three centres, they support the use of LBM CT-FFR among various practices and suggest that our findings are generalisable. Selection bias arises from the fact that the study population included only patients for whom an invasive FFR measurement was clinically indicated based on management algorithms specific to each institution, with inherent practice variations among the sites. Further studies are needed to confirm our results across various populations referred for coronary CTA. This study excluded 6% of the patients on the basis of CTA image quality. This rate can potentially be reduced with further improvements to the automated segmentation algorithm. Our findings are nonetheless generalisable, as more than 60% of the CTA examinations included in our study were performed on 64-detector row CT equipment, which is prone to misalignment artefact that can adversely affect CT-FFR accuracy when compared to single heart-beat imaging¹⁵.

Conclusions

Lattice Boltzmann-based CT-FFR has very good diagnostic accuracy to detect a significant invasive FFR ≤ 0.8 . The fast LBM CT-FFR algorithm can be performed in clinically applicable times of <60 min. The technique is highly automated and can be used as an on-site

or cloud-based service. All test characteristics of this new CT-FFR algorithm are consistent with previously reported techniques. The method is easy to use, CT vendor-independent, and has the inherent ability to scale the processing time needed to perform CT-FFR calculation to the needs of individual cardiovascular imagers.

Impact on daily practice

A newly developed and validated Lattice Boltzmann-based CT-FFR algorithm, that is CT vendor-independent, can be utilised either on-site or as a cloud-based service providing fast and accurate CT-FFR calculations.

Acknowledgements

The authors acknowledge the contributions of Drs Hiroyuki Daida, Stefania Fortini, and Giuli Jamagidze, and Mr Brian Fix to this work.

Funding

National Institutes of Health, NIBIB grant number K01-EB015868.

Conflict of interest statement

S. Melchionna is an employee of EXA Corporation. The other authors have no conflicts of interest to declare.

References

1. Taylor AJ, Cerqueira M, Hodgson JM, Mark D, Min J, O'Gara P, Rubin GD; American College of Cardiology Foundation Appropriate Use Criteria Task Force; Society of Cardiovascular Computed Tomography; American College of Radiology; American Heart Association; American Society of Echocardiography; American Society of Nuclear Cardiology; North American Society for Cardiovascular Imaging; Society for Cardiovascular Angiography and Interventions; Society for Cardiovascular Magnetic Resonance. ACCF/SCCT/ACR/AHA/ASE/ASNC/NASCI/SCAI/SCMR 2010 Appropriate Use Criteria for Cardiac Computed Tomography. A Report of the American College of Cardiology Foundation Appropriate Use Criteria Task Force, the Society of Cardiovascular Computed Tomography, the American College of Radiology, the American Heart Association, the American Society of Echocardiography, the American Society of Nuclear Cardiology, the North American Society for Cardiovascular Imaging, the Society for Cardiovascular Angiography and Interventions, and the Society for Cardiovascular Magnetic Resonance. *Circulation*. 2010;122:e525-55.
2. Cheezum MK, Hulten EA, Fischer C, Smith RM, Slim AM, Villines TC. Prognostic value of coronary CT angiography. *Cardiol Clin*. 2012;30:77-91.
3. Cheezum MK, Blankstein R. Coronary computed tomographic angiography: its role in emergency department triage. *Circulation*. 2014;130:2052-6.
4. Blankstein R, Di Carli MF. Integration of coronary anatomy and myocardial perfusion imaging. *Nat Rev Cardiol*. 2010;7:226-36.
5. Levine GN, Bates ER, Blankenship JC, Bailey SR, Bittl JA, Cercek B, Chambers CE, Ellis SG, Guyton RA, Hollenberg SM, Khot UN, Lange RA, Mauri L, Mehran R, Moussa ID, Mukherjee D, Nallamothu BK, Ting HH; ACCF; AHA; SCAI. 2011 ACCF/AHA/SCAI Guideline for Percutaneous Coronary Intervention: executive summary: a report of the American College of Cardiology Foundation/American Heart Association Task Force on Practice Guidelines and the Society for Cardiovascular Angiography and Interventions. *Catheter Cardiovasc Interv*. 2012;79:453-95.
6. Task Force Members, Montalescot G, Sechtem U, Achenbach S, Andreotti F, Arden C, Budaj A, Bugiardini R, Crea F, Cuisset T, Di Mario C, Ferreira JR, Gersh BJ, Gitt AK, Hulot JS, Marx N, Opie LH, Pfisterer M, Prescott E, Ruschitzka F, Sabaté M, Senior R, Taggart DP, van der Wall EE, Vrints CJ; ESC Committee for Practice Guidelines, Zamorano JL, Achenbach S, Baumgartner H, Bax JJ, Bueno H, Dean V, Deaton C, Erol C, Fagard R, Ferrari R, Hasdai D, Hoes AW, Kirchhof P, Knuuti J, Kolh P, Lancellotti P, Linhart A, Nihoyannopoulos P, Piepoli MF, Ponikowski P, Sirnes PA, Tamargo JL, Tenders M, Torbicki A, Wijns W, Windecker S; Document Reviewers, Knuuti J, Valgimigli M, Bueno H, Claeys MJ, Donner-Banzhoff N, Erol C, Frank H, Funck-Brentano C, Gaemperli O, Gonzalez-Juanatey JR, Hamilos M, Hasdai D, Husted S, James SK, Kervinen K, Kolh P, Kristensen SD, Lancellotti P, Maggioni AP, Piepoli MF, Pries AR, Romeo F, Rydén L, Simoons ML, Sirnes PA, Steg PG, Timmis A, Wijns W, Windecker S, Yildirir A, Zamorano JL. 2013 ESC guidelines on the management of stable coronary artery disease: the Task Force on the management of stable coronary artery disease of the European Society of Cardiology. *Eur Heart J*. 2013;34:2949-3003.
7. Di Carli MF, Murthy VL. Cardiac PET/CT for the evaluation of known or suspected coronary artery disease. *Radiographics*. 2011;31:1239-54.
8. Rochitte CE, George RT, Chen MY, Arbab-Zadeh A, Dewey M, Miller JM, Niinuma H, Yoshioka K, Kitagawa K, Nakamori S, Laham R, Vavere AL, Cerci RJ, Mehra VC, Nomura C, Kofoed KF, Jinzaki M, Kuribayashi S, de Roos A, Laule M, Tan SY, Hoe J, Paul N, Rybicki FJ, Brinker JA, Arai AE, Cox C, Clouse ME, Di Carli MF, Lima JA. Computed tomography angiography and perfusion to assess coronary artery stenosis causing perfusion defects by single photon emission computed tomography: the CORE320 study. *Eur Heart J*. 2014;35:1120-30.
9. Fihn SD, Blankenship JC, Alexander KP, Bittl JA, Byrne JG, Fletcher BJ, Fonarow GC, Lange RA, Levine GN, Maddox TM, Naidu SS, Ohman EM, Smith PK, Anderson JL, Halperin JL, Albert NM, Bozkurt B, Brindis RG, Curtis LH, DeMets D, Guyton RA, Hochman JS, Kovacs RJ, Ohman EM, Pressler SJ, Sellke FW, Shen WK; American College of Cardiology/American Heart Association Task Force on Practice Guidelines; American Association for Thoracic Surgery; Preventive Cardiovascular Nurses Association; Society for Cardiovascular Angiography and Interventions; Society of Thoracic Surgeons. 2014 ACC/AHA/AATS/PCNA/SCAI/STS focused update of the guideline for the diagnosis and management of patients with stable ischemic heart

disease: a report of the American College of Cardiology/American Heart Association Task Force on Practice Guidelines, and the American Association for Thoracic Surgery, Preventive Cardiovascular Nurses Association, Society for Cardiovascular Angiography and Interventions, and Society of Thoracic Surgeons. *J Thorac Cardiovasc Surg.* 2015;149:e5-23.

10. Tonino PA, De Bruyne B, Pijls NH, Siebert U, Ikeno F, van't Veer M, Klauss V, Manoharan G, Engström T, Oldroyd KG, Ver Lee PN, MacCarthy PA, Fearon WF; FAME Study Investigators. Fractional flow reserve versus angiography for guiding percutaneous coronary intervention. *N Engl J Med.* 2009;360:213-24.

11. Wasilewski J, Mirota K, Hawranek M, Polonski L. Invasive and non-invasive fractional flow reserve index in validation of hemodynamic severity of intracoronary lesions. *Postępy Kardiologii Interwencyjnej.* 2013;9:160-9.

12. Kakouros N, Rybicki FJ, Mitsouras D, Miller JM. Coronary pressure-derived fractional flow reserve in the assessment of coronary artery stenoses. *Eur Radiol.* 2013;23:958-67.

13. Pijls NH, Fearon WF, Tonino PA, Siebert U, Ikeno F, Bornschein B, van't Veer M, Klauss V, Manoharan G, Engström T, Oldroyd KG, Ver Lee PN, MacCarthy PA, De Bruyne B; FAME Study Investigators. Fractional flow reserve versus angiography for guiding PCI in patients with multivessel coronary artery disease: 2-year follow-up of the FAME (Fractional Flow Reserve Versus Angiography for Multivessel Evaluation) study. *J Am Coll Cardiol.* 2010;56:177-84.

14. Gewirtz H. Functional Versus Anatomic Imaging of CAD: Lessons Learned from Recent Clinical Trials. *Curr Cardiol Rep.* 2015;18:4.

15. Nørgaard BL, Leipsic J, Gaur S, Seneviratne S, Ko BS, Ito H, Jensen JM, Mauri L, De Bruyne B, Bezerra H, Osawa K, Marwan M, Naber C, Erglis A, Park SJ, Christiansen EH, Kaltoft A, Lassen JF, Bøtker HE, Achenbach S; NXT Trial Study Group. Diagnostic performance of noninvasive fractional flow reserve derived from coronary computed tomography angiography in suspected coronary artery disease: the NXT trial (Analysis of Coronary Blood Flow Using CT Angiography: Next Steps). *J Am Coll Cardiol.* 2014;63:1145-55.

16. Koo BK, Erglis A, Doh JH, Daniels DV, Jegere S, Kim HS, Dunning A, DeFrance T, Lansky A, Leipsic J, Min JK. Diagnosis of ischemia-causing coronary stenoses by noninvasive fractional flow reserve computed from coronary computed tomographic angiograms. Results from the prospective multicenter DISCOVER-FLOW (Diagnosis of Ischemia-Causing Stenoses Obtained Via Noninvasive Fractional Flow Reserve) study. *J Am Coll Cardiol.* 2011;58:1989-97.

17. Min JK, Koo BK, Erglis A, Doh JH, Daniels DV, Jegere S, Kim HS, Dunning A, DeFrance T, Leipsic J. Effect of image quality on diagnostic accuracy of noninvasive fractional flow reserve: results from the prospective multicenter international DISCOVER-FLOW study. *J Cardiovasc Comput Tomogr.* 2012;6:191-9.

18. Hlatky MA, De Bruyne B, Pontone G, Patel MR, Nørgaard BL, Byrne RA, Curzen N, Purcell I, Gutberlet M, Rioufol G, Hink U,

Schuchlenz HW, Feuchtner G, Gilard M, Andreini D, Jensen JM, Hadamitzky M, Wilk A, Wang F, Rogers C, Douglas PS; PLATFORM Investigators. Quality-of-Life and Economic Outcomes of Assessing Fractional Flow Reserve With Computed Tomography Angiography: PLATFORM. *J Am Coll Cardiol.* 2015;66:2315-23.

19. Coenen A, Lubbers MM, Kurata A, Kono A, Dedic A, Chelu RG, Dijkshoorn ML, Gijzen FJ, Ouhlous M, van Geuns RJ, Nieman K. Fractional flow reserve computed from noninvasive CT angiography data: diagnostic performance of an on-site clinician-operated computational fluid dynamics algorithm. *Radiology.* 2015;274:674-83.

20. Nickisch H, Lamash Y, Prevrhal S, Freiman M, Vembar M, Goshen L, Schmitt H. Learning Patient-Specific Lumped Models for Interactive Coronary Blood Flow Simulations. In: Navab N, Hornegger J, Wells W, Frangi A (eds). *Medical Image Computing and Computer-Assisted Intervention -- MICCAI 2015.* MICCAI 2015. Lecture Notes in Computer Science, vol 9350. Springer, Cham; 2015. p. 433-41.

21. Ko BS, Cameron JD, Munnur RK, Wong DT, Fujisawa Y, Sakaguchi T, Hirohata K, Hislop-Jambrich J, Fujimoto S, Takamura K, Crossett M, Leung M, Kuganesan A, Malaiapan Y, Nasis A, Troupis J, Meredith IT, Seneviratne SK. Noninvasive CT-Derived FFR Based on Structural and Fluid Analysis: A Comparison With Invasive FFR for Detection of Functionally Significant Stenosis. *JACC Cardiovasc Imaging.* 2017;10:663-73.

22. Taylor CA, Fonte TA, Min JK. Computational fluid dynamics applied to cardiac computed tomography for noninvasive quantification of fractional flow reserve: scientific basis. *J Am Coll Cardiol.* 2013;61:2233-41.

23. Renker M, Schoepf UJ, Wang R, Meinel FG, Rier JD, Bayer RR 2nd, Möllmann H, Hamm CW, Steinberg DH, Baumann S. Comparison of diagnostic value of a novel noninvasive coronary computed tomography angiography method versus standard coronary angiography for assessing fractional flow reserve. *Am J Cardiol.* 2014;114:1303-8.

24. Benzi R, Succi S, Vergassola M. The lattice Boltzmann equation: theory and applications. *Physics Reports.* 1992;222:145-97.

25. Chen H, Chen S, Matthaeus WH. Recovery of the Navier-Stokes equations using a lattice-gas Boltzmann method. *Phys Rev A.* 1992;45:R5339-42.

26. Qian YH, D' Humières D, Lallemand P. Lattice BGK Models for Navier-Stokes Equation. *Europhysics Letters.* 1992;17:479.

27. Rybicki FJ, Melchionna S, Mitsouras D, Coskun AU, Whitmore AG, Steigner M, Nallamshetty L, Welt FG, Bernaschi M, Borkin M, Sircar J, Kaxiras E, Succi S, Stone PH, Feldman CL. Prediction of coronary artery plaque progression and potential rupture from 320-detector row prospectively ECG-gated single heart beat CT angiography: Lattice Boltzmann evaluation of endothelial shear stress. *Int J Cardiovasc Imaging.* 2009;25:289-99.

28. Melchionna S, Amati G, Bernaschi M, Bisson M, Succi S, Mitsouras D, Rybicki FJ. Risk assessment of atherosclerotic plaques based on global biomechanics. *Med Eng Phys.* 2013;35:1290-7.

29. Melchionna S, Bernaschi M, Succi S, Kaxiras E, Rybicki FJ, Mitsouras D, Coskun AU, Feldman CL. Hydrokinetic approach to large-scale cardiovascular blood flow. *Computer Physics Communications*. 2010;181:462-72.
30. Chen H, Kandasamy S, Orszag S, Shock R, Succi S, Yakhot V. Extended Boltzmann kinetic equation for turbulent flows. *Science*. 2003;301:633-6.
31. Chen H, Teixeira C, Molvig K. Digital Physics Approach to Computational Fluid Dynamics: Some Basic Theoretical Features. *International Journal of Modern Physics C*. 1997;08:675-84.
32. Chen H, Teixeira C, Molvig K. Realization of Fluid Boundary Conditions via Discrete Boltzmann Dynamics. *International Journal of Modern Physics C*. 1998;09:1281-92.
33. Abbara S, Arbab-Zadeh A, Callister TQ, Desai MY, Mamuya W, Thomson L, Weigold WG. SCCT guidelines for performance of coronary computed tomographic angiography: a report of the Society of Cardiovascular Computed Tomography Guidelines Committee. *J Cardiovasc Comput Tomogr*. 2009;3:190-204.
34. Leipsic J, Abbara S, Achenbach S, Cury R, Earls JP, Mancini GJ, Nieman K, Pontone G, Raff GL. SCCT guidelines for the interpretation and reporting of coronary CT angiography: a report of the Society of Cardiovascular Computed Tomography Guidelines Committee. *J Cardiovasc Comput Tomogr*. 2014;8:342-58.
35. Bittencourt MS, Hulten E, Ghoshhajra B, O'Leary D, Christman MP, Montana P, Truong QA, Steigner M, Murthy VL, Rybicki FJ, Nasir K, Gowdak LH, Hainer J, Brady TJ, Di Carli MF, Hoffmann U, Abbara S, Blankstein R. Prognostic value of nonobstructive and obstructive coronary artery disease detected by coronary computed tomography angiography to identify cardiovascular events. *Circ Cardiovasc Imaging*. 2014;7:282-91.
36. Steigner ML, Mitsouras D, Whitmore AG, Otero HJ, Wang C, Buckley O, Levit NA, Hussain AZ, Cai T, Mather RT, Smedby Ö, DiCarli MF, Rybicki FJ. Iodinated contrast opacification gradients in normal coronary arteries imaged with prospectively ECG-gated single heart beat 320-detector row computed tomography. *Circ Cardiovasc Imaging*. 2010;3:179-86.
37. Paul NS, Blobel J, Kashani H, Rice M, Ursani A. Quantification of arterial plaque and lumen density with MDCT. *Med Phys*. 2010;37:4227-37.
38. Sakamoto S, Takahashi S, Coskun AU, Papafaklis MI, Takahashi A, Saito S, Stone PH, Feldman CL. Relation of distribution of coronary blood flow volume to coronary artery dominance. *Am J Cardiol*. 2013;111:1420-4.
39. Murray CD. The physiological principle of minimum work applied to the angle of branching of arteries. *J Gen Physiol*. 1926;9:835-41.
40. DeLong ER, DeLong DM, Clarke-Pearson DL. Comparing the areas under two or more correlated receiver operating characteristic curves: a nonparametric approach. *Biometrics*. 1988;44:837-45.